Pergamon

Geochimica et Cosmochimica Acta, Vol. 66, No. 21, pp. 3679–3692, 2002

0016-7037/−1898 $22.00 + .00

PII S0016-7037(01)00837-7

Catalysis by mineral surfaces: Implications for Mo geochemistry in anoxic environments

TRENT P. VORLICEK and GEORGE R. HELZ*

[1]Department of Chemistry and Biochemistry and Water Resources Research Center, University of Maryland, College Park, MD 20742, USA

(*Received April* 13, 2001; *accepted in revised form October* 12, 2001)

Abstract—Fixation of Mo in sulfidic environments is believed to be preceded by conversion of geochemically passive MoO_4^{2-} to particle-reactive thiomolybdates ($MoO_xS_{4-x}^{2-}$). In aqueous solution, these transformations are general-acid catalyzed, implying that proton donors can accelerate both the forward and reverse reactions. Here, we explore whether mineral surfaces also catalyze thiomolybdate interconversions. The rate of MoS_4^{2-} hydrolysis is investigated in the presence and absence of natural kaolinite (KGa-1b) and synthetic Al_2O_3 and SiO_2 phases. Comparison of rates achieved with these phases suggests that the Al oxyhydroxide component in kaolinite furnishes the catalytic activity. An anhydrous Al_2O_3 phase is catalytically inactive until hydrated (and therefore protonated). Surface kinetics with kaolinite at mildly alkaline pH are consistent with rate limitation by formation or decomposition of monomeric surface complexes; oligomeric surface intermediates may become important at $MoS_4^{2-} > 20$ μmol/L, higher than is likely to be found in nature. The pH dependence of the kaolinite-catalyzed reaction suggests that weak-acid surface sites promote hydrolysis. Intermediate thiomolybdates or molybdate appears to compete for active sites, inhibiting MoS_4^{2-} hydrolysis. Catalysis of $MoOS_3^{2-}$ hydrolysis is also observed but has not been studied systematically. Thiomolybdate hydrolysis is inhibited slightly by sulfate and more strongly by phosphate. Low NaCl concentrations ($<10^{-2}$ mol/L) promote hydrolysis, but higher NaCl concentrations retard the reaction to a small extent. A mechanism is postulated involving expansion of the coordination number around Mo from 4 to 6 under the influence of the surface. The effective concentration of surface sites available to Mo in sediment pore waters is likely to be large enough to greatly accelerate thiomolybdate hydrolysis and sulfidation. Possibly this explains why Mo capture in seasonally or intermittently anoxic environments often occurs through processes operating within sediments but not in overlying waters.

We seem to be stymied in our quest for a precise definition of the trace-metal chemistry of Phanerozoic seawater, and we will probably remain so until we know more about the processes that control the trace metal enrichment of black shales. (Holland, 1984, p. 498)

1. INTRODUCTION

The Mo concentrations in sediments and sedimentary rocks that form in anoxic environments preserve useful information about local redox conditions at the time of sediment formation (e.g., Dean et al., 1997, 1999; Crusius et al., 1999; Zheng et al., 2000; Yarincik et al., 2000; Adelson et al., 2001). Molybdenum concentrations may also place constraints on the average global redox state of the ocean over geologic time (Holland, 1984; Emerson and Huested, 1991; Morford and Emerson, 1999). Unfortunately, an incomplete understanding of deposition mechanisms has hampered interpretation of Mo records.

X-ray spectroscopic evidence from black shales and from laboratory-generated scavenging products led Helz et al. (1996) to propose that a key step in Mo scavenging from seawater was conversion of particle-inert MoO_4^{2-} to particle-reactive thiomolybdates ($MoO_xS_{4-x}^{2-}$, x = 0 to 3). Thiomolybdates were scavenged readily from solution by sulfidized Fe phases and humic materials; at the molecular scale, laboratory-produced products resembled those found in black shales. Erickson and Helz (2000) used thermodynamic and kinetic evidence to argue that two limits to thiomolybdate production and thus Mo scavenging would be (a) H_2S(aq) concentration, which must exceed ~11 μmol/L at 25°C, and (b) time of exposure of MoO_4^{2-} to H_2S. Without assistance from catalysts, formation of higher thiomolybdates, $MoOS_3^{2-}$ and MoS_4^{2-}, would be too slow to proceed significantly in seasonally sulfidic waters. Erickson and Helz (2000) conjectured that reactions at mineral surfaces in sediments might circumvent the kinetic barrier because of surface catalysis. This could explain why Mo fixation appears to occur within sediments more readily than in overlying water in seasonally or intermittently sulfidic environments (Francois, 1988; Colodner, 1991; Zheng et al., 2000; Adelson et al., 2001).

In this paper, we test the conjecture that mineral surfaces are effective molybdate and thiomolybdate catalysts. Our study focuses on kaolinite ($Al_2Si_2O_5[OH]_4$), a common clay mineral that typically accounts for 8 to 20% of marine sediments (Griffin et al., 1968). We selected kaolinite because it is unreactive to sulfide (unlike many transition metal oxides) and because well-characterized material with high specific surface area is readily available. We have no reason to believe that kaolinite would be the only mineral catalyst or the most important one in nature.

We restrict our investigation to the hydrolysis of MoS_4^{2-}, which would have a half-life of decades at neutral pH if uncatalyzed (Erickson and Helz, 2000). Because successive hydrolysis reactions (i.e., $MoS_4^{2-} \rightarrow MoOS_3^{2-} \rightarrow MoO_2S_2^{2-} \ldots$) increase in rate, hydrolysis products accumulate minimally in solution, simplifying interpretation of ultraviolet-visible (UV-vis) spectra. When these reactions are studied in the direction of sulfidation, each successive step is slower, and accumulating

* Author to whom correspondence should be addressed (gh17@umail.umd.edu).

products complicate the spectra. All catalysts comparably accelerate forward and reverse rates of elementary reactions. Under near-equilibrium conditions, the rate of sulfidation can be estimated from knowledge of the rate of hydrolysis by applying the principle of detailed balance (Laidler, 1987, p. 130).

Although this paper deals with Mo geochemistry, our findings concerning catalytic mechanisms at clay mineral surfaces have broader implications regarding clay mineral–catalyzed reactions in nature. Kaolinite has been shown to catalyze amino acid condensation, possibly an important step in the origin of life (Zamaraev et al., 1997). Kaolinite catalyzes condensation of hydroquinone in near-neutral solutions to produce humic-like polymers (Wang and Huang, 1989). Kaolinite catalyzes hydrolysis of pyrophosphate and various anthropogenic organic compounds (Saltzman et al., 1974; Mingelgrin et al., 1977; Mingelgrin and Saltzman, 1979; El-Amamy and Mill, 1984; Al-Kanani and MacKenzie, 1990; Xu, 1998).

2. CONCEPTUAL FRAMEWORK

Rates of many kinds of reactions in aqueous solution are found to vary with pH as described by the general rate law:

$$\text{Rate} = \pm [X][Y][k_H(H_3O^+) + k_N(H_2O) + k_{OH}(OH^-) + k_{HB}(HB) + k_B(B^-)]. \quad (1)$$

Here, X and Y are the concentrations of two reactants, HB is the concentration of the protonated form of a buffer, and B^- is the concentration of the deprotonated form of a buffer. In this discussion, we assume that H_3O^+, H_2O, OH^-, HB, and B^- are not consumed in the reaction and therefore are catalysts by definition (since they affect the reaction rate according to the equation). Clearly, which term within the final set of brackets in Eqn. 1 dominates depends on solution composition. In any particular reaction, some of the terms usually are found to be immeasurably small regardless of solution composition.

Studies of molybdate and thiomolybdate transformations in homogeneous solution have shown that these reactions are subject to general-acid catalysis (Brule et al., 1988; Erickson and Helz, 2000). In other words, under the conditions of those studies, it was possible to quantify k_H, k_N and k_{HB} for various buffers. No evidence of base catalysis, characterized by k_{OH} and k_B terms, was observed. It was further shown that these rate constants were linked through the Brønsted relationship, in which the coefficient, 0.5, is an empirical constant:

$$\log \frac{k_{HB_1}}{k_{HB_2}} = -0.5(pK_{a1} - pK_{a2}). \quad (2)$$

By employing $pK_a = -1.7$ for H_3O^+ and $pK_a = 15.5$ for H_2O, k_H and k_N can be included in this correlation (see Jencks, 1969, p. 170 ff for a discussion). As this relationship indicates, stronger acids (lower pK_a values) are associated with faster rate constants.

Erickson and Helz (2000, Fig. 8) showed that formation and decomposition of MoS_4^{2-} and $MoOS_3^{2-}$ would be slow on the time scale of seasonal anoxic events in coastal waters in the absence of catalysts other than H_3O^+, HCO_3^-, and H_2O. To account for Mo fixation in seasonally anoxic systems, they invoked buffer catalysts operating below the sediment-water interface. However, Perdue and Wolfe (1983) pointed out that even in sediment pore waters, concentrations of dissolved, weak-acid proton donors (e.g., NH_4^+, $H_2PO_4^-$, fulvic acid) are probably too low to make these catalysts significant in general-acid catalyzed reactions such as the molybdate and thiomolybdate transformations.

Proton donors associated with mineral surfaces may offer a way to circumvent the problem raised by Perdue and Wolfe (1983). Hydrated oxide and silicate surfaces consist largely of $\equiv$M-OH_2^+, $\equiv$M-OH^0, and $\equiv$M-O^- groups. Acidities of the $\equiv$M-OH_2^+ and $\equiv$M-OH^0 groups are only moderate. For various oxides, intrinsic pK_a values (i.e., pK_a values that would be exhibited on an uncharged surface) range from 3 to 7 for $\equiv$M-OH_2^+ and from 6 to 10 for $\equiv$M-OH^0 (Schindler and Stumm, 1987). However the kinetic significance of proton donors depends on both their K_a values and their concentrations. Within sediments, the concentration of surface acid sites per unit volume of aqueous solution is potentially large. This is shown in Figure 1, which is based on surface site densities reasonable for kaolinite (Goldberg et al., 1998). Figure 1 shows that fine-grained, suspended particles in rivers, lakes, and the ocean are expected to provide only submicromolar concentrations of sites for catalysis. On the other hand, within pore waters of recent, fine-grained sediments, site concentrations of 1 to 100 mmol/L can be achieved. Mineral surfaces are likely to be the dominant proton donors available to solutes in pore waters.

While the proton-donating capacity of mineral surfaces can be important, it must be remembered that surface catalysis is a more complex process controlled partly by orientation and structural modification of adsorbed reactants before reaction. Molybdate and thiomolydate transformations are an ideal system in which to explore surface catalysis because (a) they are easily monitored optically; (b) they react at convenient rates; and (c) they adsorb negligibly at near-neutral pH, implying that reaction products will block reactive surface sites minimally.

3. EXPERIMENTAL METHODS

The Clay Mineral Society standard KGa-1b was purchased from the University of Missouri–Columbia Source Clay Repository and used without pretreatment. KGa-1b is a well-crystallized kaolinite from Washington County, Georgia (Pruett and Webb, 1993; Sutheimer et al., 1999). Halloysite (a polymorph of kaolinite) has been found to be a trace component of KGa-1b (Zhou, 1996). Trace amounts of TiO_2 (1.64% w/w), Fe_2O_3 (0.21% w/w), quartz, micas, alkali, and alkaline earth oxides are also present in the source kaolin (Pruett and Webb, 1993). KGa-1b has a Brunauer-Emmett-Teller (BET) surface area of 12.5 m^2/g (Bereznitski et al., 1998) and point of zero net proton condition of 5.1 $\pm$ 0.2 (Sutheimer et al., 1999).

δ-Al_2O_3 (Aluminium Oxid C) and silica (Aerosil 200) were acquired from the Degussa Corporation. δ-Al_2O_3 has a reported BET surface area of 102.9 m^2/g and point of zero charge of 9.30 (Goldberg et al., 1998). The silica product has a BET surface area of 182 m^2/g and point of zero charge of 2.4 (Young, 1981).

The following reagents were purchased and used as received: $Na_2B_4O_7 \cdot 10H_20$ (J. T. Baker), NaCl (J. T. Baker), $NaH_2PO_4 \cdot H_2O$ (J. T. Baker), Na_2SO_4 (Fisher), and $(NH_4)_2MoS_4$ (Strem). All solutions were prepared from >18 M$\Omega \cdot$ cm resistivity water (B-Pure, Barnstead). Glassware was soaked in 5% HNO_3 and rinsed thoroughly with deionized water before use.

Although the ammonium salt of tetrathiomolybdate is commercially available, the sodium salt was used for these experiments because of the possibility that NH_4^+ could act as a proton-donating catalyst. The procedure for synthesizing $Na_2MoS_4 \cdot 3.5H_2O$ followed Laurie et al. (1984). An ice-cooled 2-mol/L NaOH solution was deoxygenated with

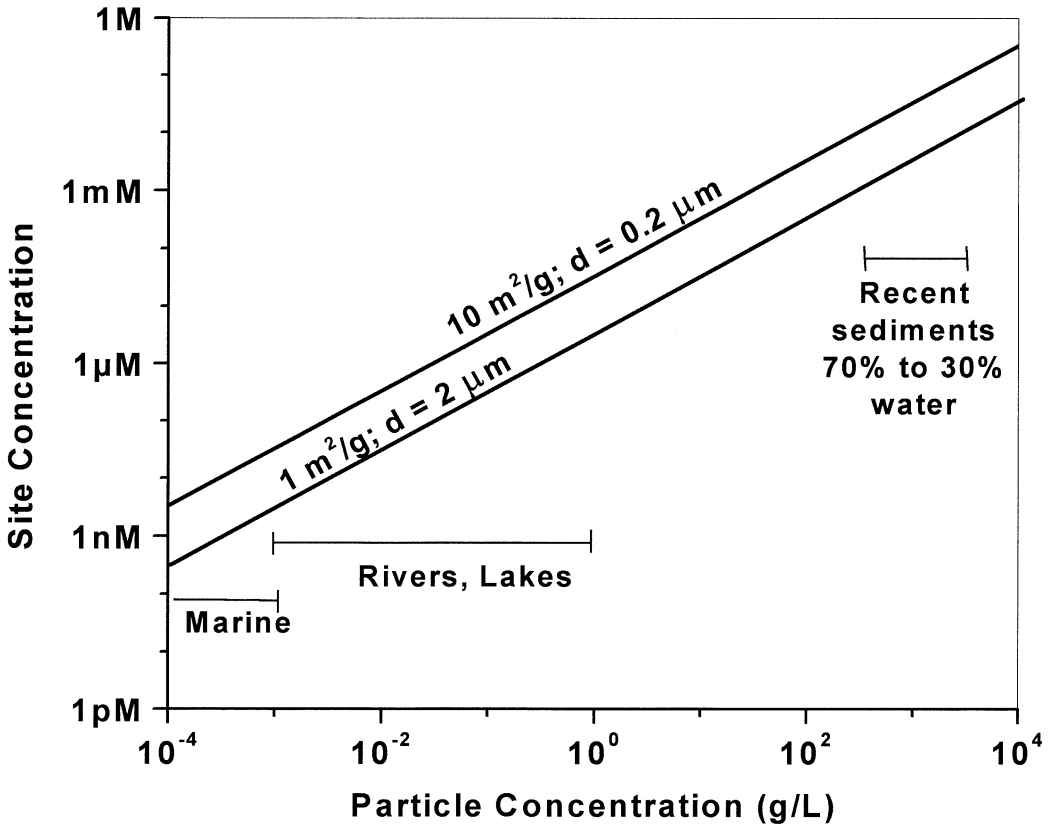

Fig. 1. Site concentrations in moles of sites per liter of water as a function of particle concentrations for solids having specific surfaces of 10 m^2/g and 1 m^2/g and surface site densities of 2 sites/nm^2. Nominal particle diameters (d) assume spherical, monodisperse particles of 2.75 g/cm^3 density.

N_2 (≈1 h) and immediately passed into an N_2-filled glove box. Twenty milliliters of the NaOH solution were added to a 50-mL round-bottom flask containing 5.00 g $(NH_4)_2MoS_4$. After mixing, the resulting solution was syringe filtered (0.45 μm) into a 50-mL vacuum flask. NH_3 and H_2O were slowly removed by vacuum evaporation. The residue was extracted with 60 mL of deoxygenated acetone and gravity filtered. Blood-red crystals of the product formed upon addition of 150 mL of deoxygenated ether. The crystals were gravity filtered, washed with ether, and dried in an evacuated desiccator. A typical yield for this synthesis was 80%. Storage of the salt in an oxygen and water free atmosphere is imperative. Otherwise, the soluble blood-red crystalline salt slowly degrades into an insoluble, X-ray amorphous, black solid.

The pH of test solutions and slurries was controlled using borate buffering. Borate is a favorable choice because of its poor Brønsted acid character (i.e., weak homogeneous acid catalysis) and mildly alkaline buffering range. Higher concentrations of borate were found to retard hydrolysis rates (implying competition of $B(OH)_4^-$ with MoS_4^{2-} for active sites), but below 2 mmol/L, rates were independent of borate. Experimentally convenient rates were obtained with B_T = 0.8 mmol, where B_T is the total dissolved plus adsorbed boron species. This concentration was used for all experiments involving borate buffering.

Unless otherwise noted, preparation of test solutions and slurries followed a 2 day regimen. On the first day, borate buffer solutions were prepared using $Na_2B_4O_7 \cdot 10H_2O$. NaCl, Na_2SO_4, or $NaH_2PO_4 \cdot H_2O$ was added to the buffer for experiments involving these salts. Kinetic experiments were conducted in flasks containing 250 mL of buffer solution plus an appropriate amount of test solid. The pH of the magnetically stirred solution and slurry was adjusted using either HCl or NaOH. After adjusting to the experimental pH, the flasks were capped, and the slurry was allowed to age overnight to ensure hydration of the solid surfaces.

On the second day, the pH of the slurry and solution was measured and, if necessary, adjusted again. The solution and suspension were bubbled for a minimum of 1 h with N_2 deoxygenated by a Ridox (Fisher) column. The vessels were capped and immediately passed into an N_2-filled glove box. Once inside the glove box, the kaolin or oxide particles were kept suspended by magnetic stirring. A cork stand was placed between the vessel and magnetic stirrer to minimize heat transfer. Aliquots of ≈0.01 mol/L MoS_4^{2-} stock solution (standardized by UV-vis spectroscopy) were added to the reaction flasks. The temperature for these experiments varied within the range from 21 to 23°C.

At various times, aliquots of the reaction solution and slurry were filtered into plastic centrifuge tubes using 0.45-μm syringe filters (Whatman). Kaolin or oxide filtrates were further filtered with 0.02-μm syringe filters (Whatman) to eliminate any remaining particles. The tubes were capped and passed out of the glove box. After measuring the pH of the samples, UV-vis absorption spectra were recorded. The samples were then frozen and saved for total Mo analysis using atomic absorption spectroscopy.

All pH measurements were made with an Orion model 420A meter equipped with an Orion model 8103 combination microelectrode. The meter was calibrated between pH 7 and 10 with commercial buffers. MoS_4^{2-} hydrolysis reactions were monitored by UV-vis absorption spectroscopy (1.00-cm quartz cuvette) vs. a deionized water blank solution. MoS_4^{2-} absorbance was monitored at 468 nm ($\varepsilon_{\lambda 468}$ = 11,870 mol/L^{-1} cm^{-1}). When necessary, $MoOS_3^{2-}$ was quantified using the absorbance at 396 nm ($\varepsilon_{\lambda 396}$ = 9030 mol/L^{-1} cm^{-1}), at which MoS_4^{2-} does not absorb appreciably. The contribution of $MoOS_3^{2-}$ to the total absorbance at 468 nm was calculated and MoS_4^{2-} absorbance obtained by difference.

Total molybdenum was determined by flame (N_2O-C_2H_2) atomic absorption on a Perkin-Elmer model 5000 spectrophotometer at a wavelength of 313.3 nm. The method employed is the same as that of Erickson (1997). Standard curves were produced between 0.5 and 20

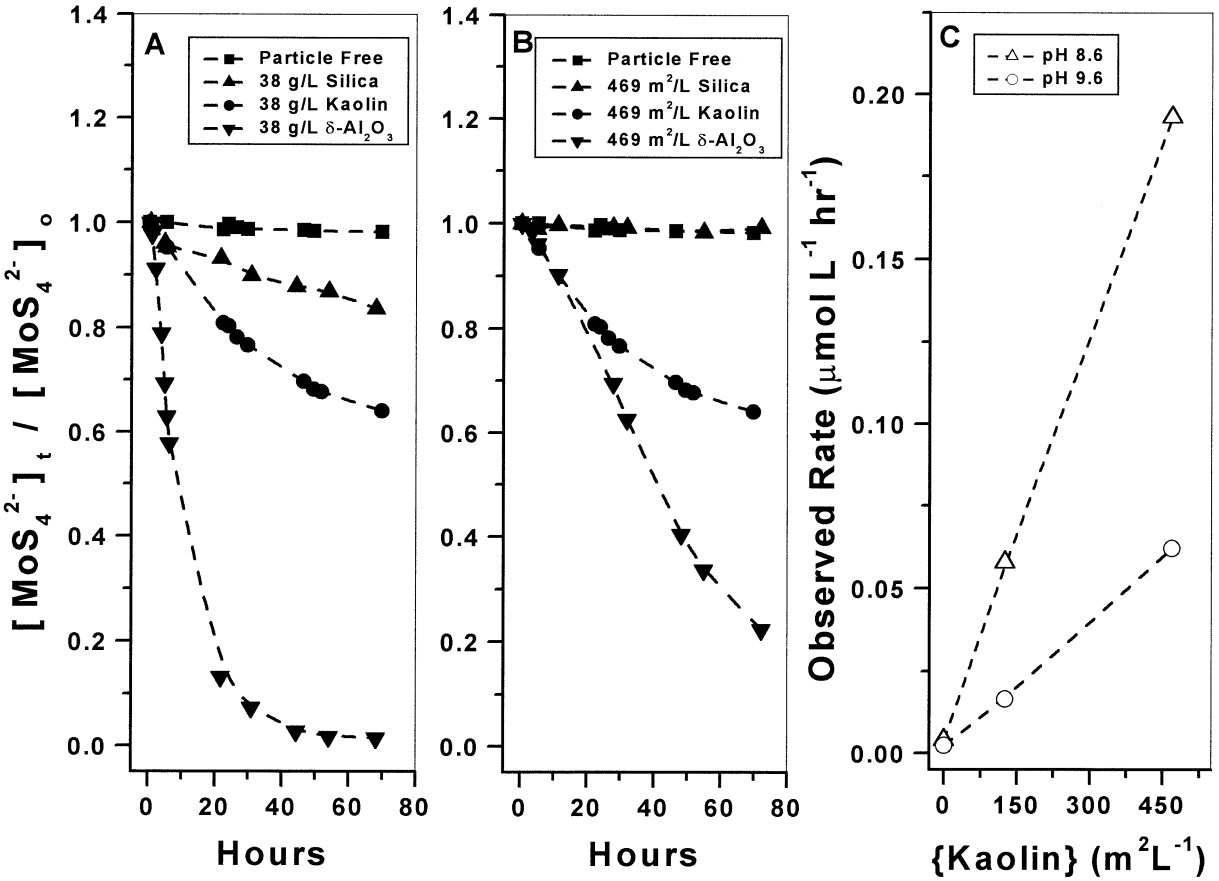

Fig. 2. Comparison of MoS_4^{2-} hydrolysis curves for particle-free solution and suspensions of SiO_2, kaolin, and hydrated δ-Al_2O_3 at (A) constant mass loading and (B) constant areal concentration, both at pH 8.6. (C) The effect of kaolin concentration on the observed initial rate of MoS_4^{2-} hydrolysis at pH 8.6 and 9.6. Homogenous conditions for (A), (B), and (C): MoS_4^{2-} (initial) = 18 μmol/L; B_T = 0.8 mmol/L; I = 0.9 mmol/L.

ppm Mo. Al (1000 ppm) and BrCl (0.9 mmol/L) were added to all standards and samples. The presence of Al is required to eliminate interference from sulfate, phosphate, and iron (David, 1968). Before addition of Al, BrCl was added to oxidize sulfide to sulfate, preventing precipitation of aluminum sulfide. BrCl is prepared by dissolving KBr and $KBrO_3$ in concentrated HCl. The detection limit for Mo using this technique is 0.2 ppm ($\approx$2 μmol/L).

Leachable phosphate in KGa-1b was determined to assess its importance in self-inhibition of reactions at the kaolin surface. The surface was first cleaned (Sutheimer et al., 1999), and then a suspension of 100 g kaolin in 500 mL 1 mol/L NaCl adjusted to pH 3 was prepared and magnetically stirred for 4 h. After settling overnight, aliquots of the supernatant were taken. Phosphate was quantified according to the vanadomolybdophosphoric acid colorimetric method (Greenberg et al., 1992).

4. RESULTS

4.1. MoS_4^{2-} Hydrolysis in Particle-Free Solution vs. Oxide Suspensions

Examples of MoS_4^{2-} hydrolysis experiments are shown in Figure 2. Enhanced rates of MoS_4^{2-} hydrolysis in the presence of silica, δ-Al_2O_3, and kaolin are demonstrated in Figure 2a, which compares the three test solids at the same mass concentration. At pH 8.6, the initial rates of hydrolysis increase by factors of approximately 10, 35, and 340 relative to particle-free solution for 38 g/L suspensions of silica, kaolin, and hydrated δ-Al_2O_3, respectively. Figure 2b compares the same test solids when mass concentrations are adjusted so that the surface concentration of each solid is 469 m^2/L. In this case, hydrolysis rates for the silica suspension and particle-free solution are indistinguishable. In contrast, kaolin and hydrated δ-Al_2O_3 have similar initial rates. This comparison suggests that the Al-oxyhydroxide component of kaolinite furnishes most of this mineral's catalytic activity. Figure 2c shows that kaolinite's acceleration of the initial rate at pH 8.6 and 9.6 is a linear function of the kaolinite surface area per unit volume of solution, indicating first-order kinetics with respect to surface concentration.

As expected, in the absence of solids in suspension, intermediate thiomolybdate species are not observed because of their successively faster rates of hydrolysis. Because the ultimate product, MoO_4^{2-}, does not absorb light above 230 nm, the MoS_4^{2-} absorption spectrum uniformly collapses in particle-free solution as hydrolysis proceeds (Clarke and Laurie, 1987). In contrast, Figure 3 shows the typical spectral changes occurring in the solution in the presence of catalytically active concentrations of kaolin, hydrated δ-Al_2O_3, or silica. As the MoS_4^{2-} peaks centered around 318 and 468 nm collapse, a peak

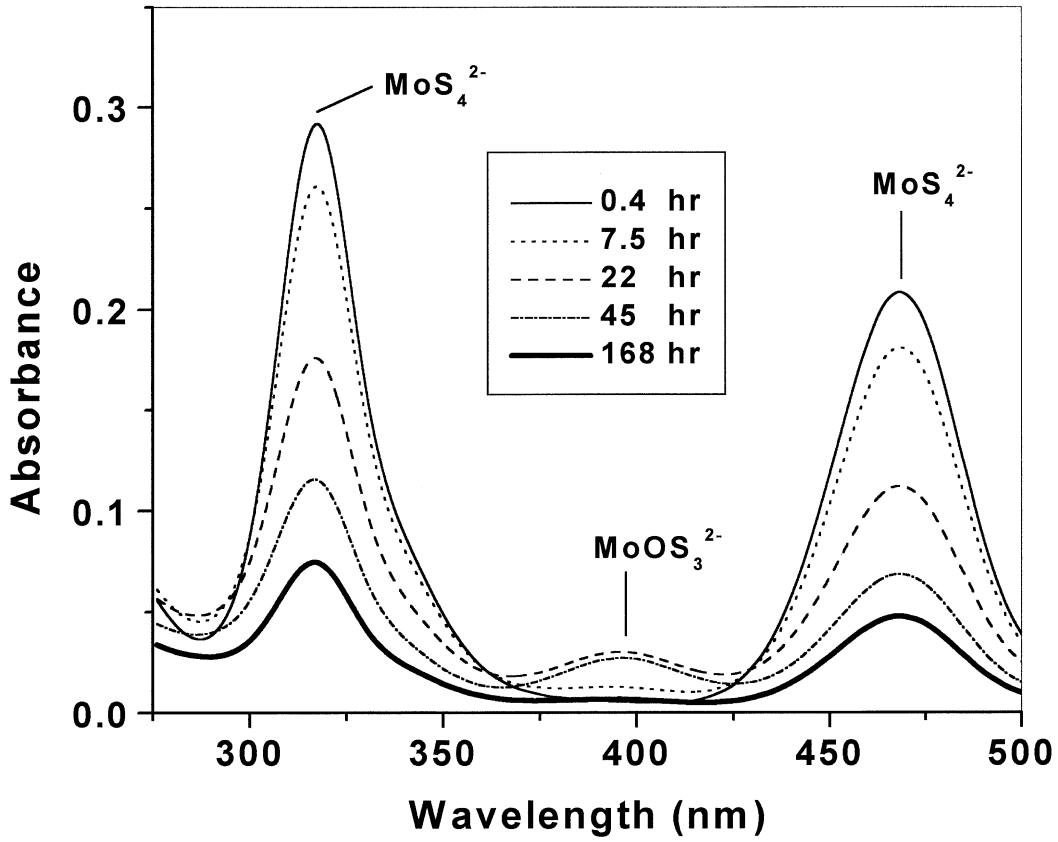

Fig. 3. Typical spectral changes occurring over the course of an experiment involving either kaolin, δ-Al_2O_3, or SiO_2 suspensions. Peaks centered around 318 and 468 nm are associated with MoS_4^{2-}; the peak centered at 396 nm is attributed to $MoOS_3^{2-}$ (Erickson and Helz, 2000). Conditions: MoS_4^{2-} (initial) = 18 μmol/L; B_T = 0.8 mmol/L; pH = 8.6; {kaolin} = 469 m^2/L; I = 3 mmol/L (NaCl).

centered around 396 nm rises to a maximum. Finally, the three peaks collapse together. The peak with a maximum at 396 nm is attributed to $MoOS_3^{2-}$. Contributions of $MoO_2S_2^{2-}$ or MoO_3S^{2-} to the spectra are negligible.

Visible accumulation of $MoOS_3^{2-}$ during the surface-catalyzed hydrolysis of MoS_4^{2-} indicates the MoS_4^{2-} to $MoOS_3^{2-}$ hydrolysis step is catalyzed to a greater extent than the $MoOS_3^{2-}$ to $MoO_2S_2^{2-}$ step. $MoO_2S_2^{2-}$ and MoO_3S^{2-} are not observed because their homogenous hydrolysis rates are too fast. The variation in rates for the thiomolybdate hydrolysis sequence points to a selective interaction between thiomolybdate anions and surface sites.

4.2. Effect of Hydrating δ-Al_2O_3 on MoS_4^{2-} Hydrolysis

Figure 4 compares MoS_4^{2-} hydrolysis curves for 38 g/L anhydrous and hydrated δ-Al_2O_3 suspensions. The figure demonstrates that anhydrous δ-Al_2O_3 is negligibly active as a catalyst until it has experienced a few hours of equilibration with water. When the δ-Al_2O_3 is pre-equilibrated in water before adding MoS_4^{2-}, catalytic activity commences immediately. Scanning electron microscopy pictures (Vorlicek, in preparation) show a morphologic change in δ-Al_2O_3 particles during hydration. Untreated δ-Al_2O_3 exhibits a mostly uniform spherical shape. Upon aging in water, the particles become irregular and angular, although they do not change noticeably in average size. Eng et al. (2000) reported that hydrated α-Al_2O_3 is an intermediate between α-Al_2O_3 and γ-$Al(OH)_3$. A comparable structural change must occur for δ-Al_2O_3 during hydration.

The catalytic significance of hydration probably lies in the creation of surface sites capable of becoming proton donors. Catalysis exhibited in aged slurries is not due to dissolved components leached from the δ-Al_2O_3. The open circles in Figure 4 show that little MoS_4^{2-} loss occurs over 2 d in the supernatant of an aged δ-Al_2O_3 suspension.

4.3. MoS_4^{2-} Hydrolysis in Kaolin Suspensions

Figure 5 compares hydrolysis rates for two 38-g/L suspensions of kaolin in different ionic media: NaCl vs. Na_2SO_4, both at an ionic strength of 3 mmol/L. Hydrolysis in the sulfate medium is distinctly slower. Note that $MoOS_3^{2-}$ accumulates as the rate of MoS_4^{2-} loss slows. The right panel of Figure 5 includes some atomic absorption data, which demonstrate that within uncertainty, total dissolved molybdenum remains constant over the course of the reaction involving Na_2SO_4. This is consistent with expectations, since MoO_4^{2-} adsorbs negligibly to kaolinite above pH 7 (Goldberg et al., 1998) and since

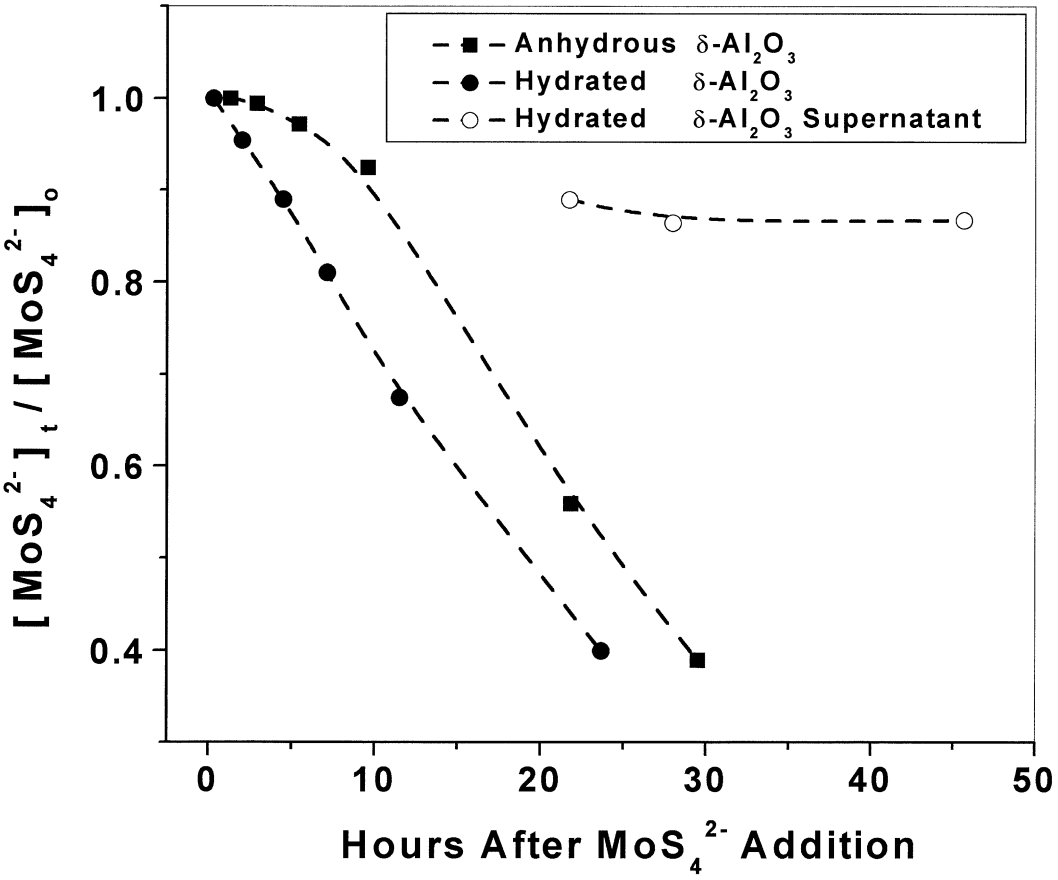

Fig. 4. Comparison of MoS_4^{2-} hydrolysis curves for 38-g/L slurries of anhydrous and hydrated δ-Al_2O_3 and the supernatant of a 38-g/L hydrated δ-Al_2O_3 suspension at pH 9 and 18 μmol/L initial MoS_4^{2-}. *Anhydrous* means the slurry was prepared minutes before addition of MoS_4^{2-}. *Hydrated* means the suspension was prepared and allowed to equilibrate for 2 d before addition of MoS_4^{2-}. *Supernatant* refers to a solution from which δ-Al_2O_3 had been removed by filtration (0.45 μm) before MoS_4^{2-} addition. The supernatant may have contained some colloidal-sized δ-Al_2O_3 particles. No additional salt or buffer was added for ionic strength or pH control.

replacement of O by S in the first coordination sphere should further decrease the affinity of Mo for aluminosilicate surfaces.

The slowdown of MoS_4^{2-} hydrolysis rate shown in Figure 5 is representative of all experiments involving kaolin. This cannot be explained by back reaction of $MoOS_3^{2-}$ to MoS_4^{2-} because this reaction would be too slow and thermodynamically unfavored at the prevailing HS^- concentrations. The observation suggests that either intermediate thiomolybdates or molybdate compete for active sites on the clay surface, reducing the efficiency of further hydrolysis. The retarding effect of SO_4^{2-} compared to Cl^- can also be understood in terms of competition of the oxyanion for active sites on the kaolin surface. Figure 5 shows that $MoOS_3^{2-}$ hydrolysis, like that of MoS_4^{2-}, is retarded by sulfate.

4.4. Kinetics of MoS_4^{2-} Hydrolysis in Kaolin Suspensions

In these experiments, the total rate of thiomolybdate loss by hydrolysis must be regarded as due to reactions along both aqueous-phase and surface-mediated pathways:

$$\text{Observed Rate} = [k_H(MoS_4^{2-})(H_3O^+) + k_N(MoS_4^{2-})(H_2O) + k_{HB_1}(MoS_4^{2-})(HB_1) + \ldots] + [\Sigma(A)f_{(H_3O^+,\,MoS_4^{2-})}], \quad (3)$$

where A is the solid surface concentration (m^2/L) and $f_{(H_3O^+,MoS_4^{2-})}$ is a function, to be determined below, of pH and thiomolybdate concentration. The summation acknowledges the possibility of multiple reaction pathways on the kaolinite surface.

We now define an experimentally determinable specific surface rate (R^*) as follows:

$$R^* = \frac{[\text{observed rate} - \text{aqueous-phase rate}]}{A} = \Sigma f_{(H_3O^+,\,MoS_4^{2-})}. \quad (4)$$

In principle, the aqueous-phase rate could be calculated using the data of Erickson and Helz (2000), but here, we will use our own measurements of this rate in particle-free solution. Some error may be introduced into the value of R^* owing to differences in pH between the particle-bearing and particle-free solutions, but this error should be small because pH was usually matched to ± 0.1. Also, aqueous-phase rates are at least an order of magnitude lower than observed rates, so uncertainty in aqueous-phase rates has greatly diminished influence on uncertainty in R^*. For A, we will use the BET surface area of 12.5 m^2/g (Bereznitski et al., 1998). Because R^* is calculated from

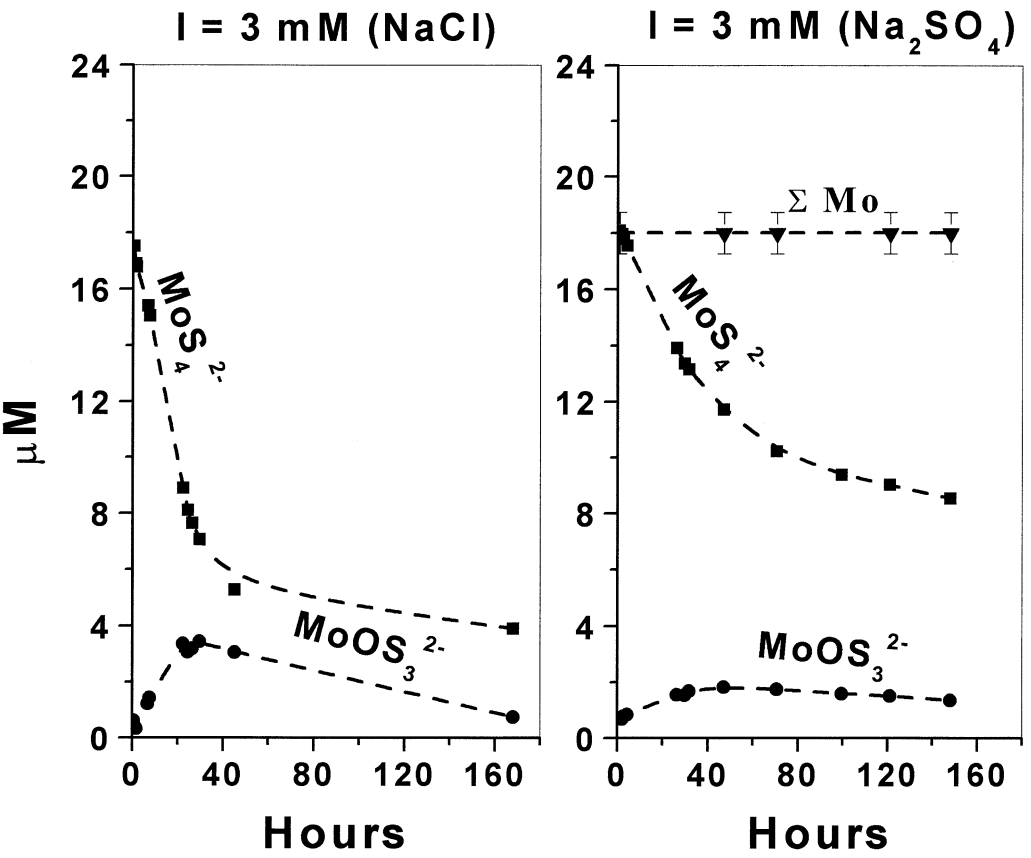

Fig. 5. Mo speciation as a function of time for two 38-g/L kaolin suspensions containing NaCl or Na_2SO_4 at equivalent ionic strengths. ΣMo was quantified only for the Na_2SO_4 slurry. Error bars are the standard deviation for ΣMo calculated from an atomic absorption calibration curve. Conditions for both figures: MoS_4^{2-} (initial) = 18 μmol/L; B_T = 0.8 mmol/L; pH = 8.6; {kaolin} = 469 m^2/L.

initial rates of hydrolysis, it is important to note that R^* reflects the areal rate of MoS_4^{2-} hydrolysis before retarding influences by intermediate thiomolybdates or MoO_4^{2-}, as inferred from Figure 5.

The dependence of R^* on pH is exhibited in Figure 6. The data appear to fall into two distinct groups. At pH < 8.8, the data show similar R^* values of $\sim 4 \times 10^{-4}$ μmol h^{-1} m^{-2}. At pH > 9.5, R^* is $\sim 1.5 \times 10^{-4}$ μmol h^{-1} m^{-2}. Note that surface catalysis exists throughout the pH range investigated; in the absence of surface catalysis, R^* would equal zero.

The relationship displayed in Figure 6 suggests that there are at least two reaction pathways responsible for surface-enhanced hydrolysis. One pathway deactivates as pH is raised above ~9, presumably because an active site on the kaolinite surface loses a proton. Since the reaction rate ascribed to each pathway differs by only about threefold, presumably, both pathways contribute significantly to the total hydrolysis rate below pH 9.

Figure 7 shows the dependence of the specific surface rate on initial MoS_4^{2-} concentration at pH 9.6 and 8.6, representing the two pH regimes indicated in Figure 6. At pH 9.6 (Fig. 7a), R^* was calculated according to Eqn. 4. For Figure 7b, R^* values were further corrected for the contribution of the pH > 9 pathway to the rate at pH < 9; this correction was made as follows:

$$R^{\ddagger} = R^*\,(\text{pH } 8.6) - R^*\,(\text{pH } 9.6). \tag{5}$$

By treating rates in this manner, the left- and right-hand panels of Figure 7 reflect the rate dependence on MoS_4^{2-} for only the dominant pathway in each of the two pH regimes delineated in Figure 6.

Data for both pH regimes were fit using two alternative models. The first model, represented by the solid lines in Figure 7, is described by the following equation:

$$R^* = \frac{R^*_m\,[MoS_4^{2-}]}{k_{1/2} + [MoS_4^{2-}]}\ (\text{constant pH}). \tag{6}$$

This equation contains two parameters, R^*_m and $K_{1/2}$. R^*_m is the maximum rate of hydrolysis achievable by a surface pathway, and $K_{1/2}$ (value of $[MoS_4^{2-}]$ at $R^*_m/2$) is a measure of the affinity of surface sites for MoS_4^{2-}. The equation for $R^{\ddagger}$ at pH 8.6 is identical in form to Eqn. 6. Eqn. 6 assumes that the reactive intermediate is a monomeric surface complex formed through the following equilibrium:

$$\equiv S + MoS_4^{2-} \leftrightarrow \equiv S - (MoS_4^{2-}). \tag{7}$$

Nonlinear regression on the data at pH 8.6 gives $R^{\ddagger}_m = 20 \times 10^{-4}$ μmol h^{-1} m^{-2} and $K_{1/2}$ = 250 μmol/L. For pH 9.6, $R^*_m = 3 \times 10^{-4}$ μmol h^{-1} m^{-2} and $K_{1/2}$ = 20 μmol/L. At both pHs, both fitted parameters have large uncertainties (>50%).

Inspection of the fits in Figure 7 suggests systematic devia-

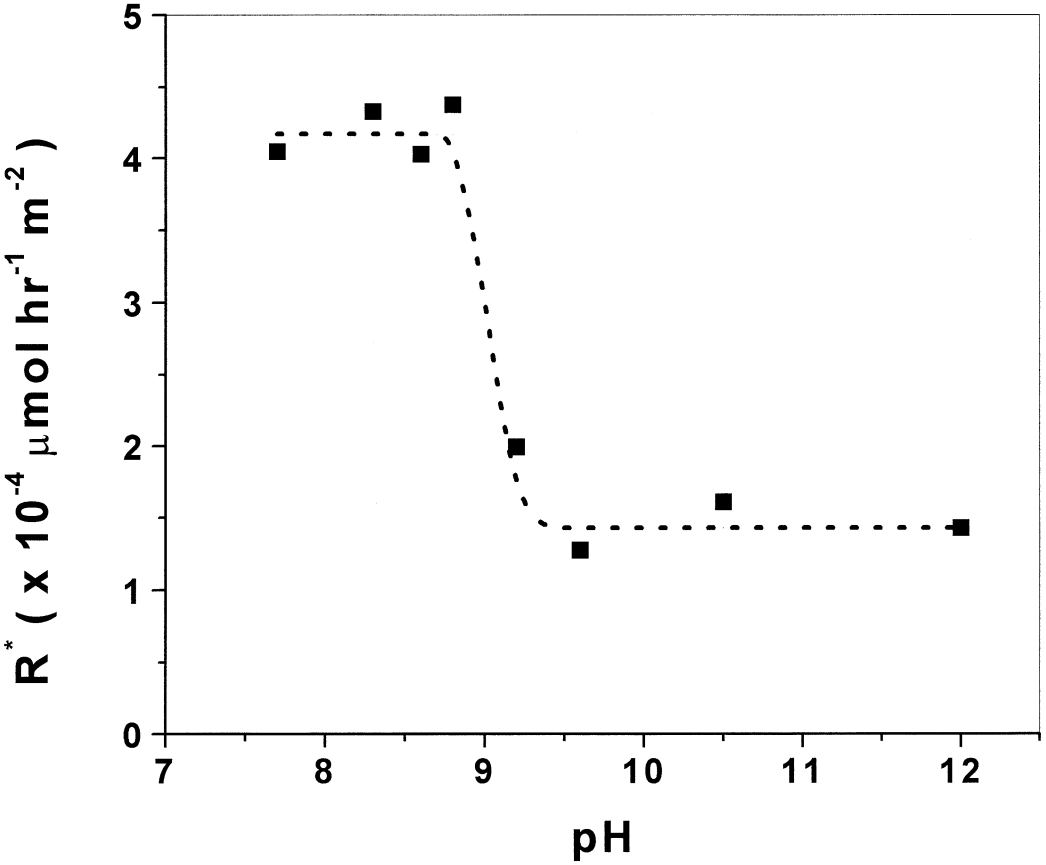

Fig. 6. The effect of pH on R^*, which is defined by Eqn. 4 in the text. Conditions: MoS_4^{2-} (initial) = 18 μmol/L; B_T = 0.8 mmol/L; {kaolin} = 469 m^2/L; I $\approx$ 1 mmol/L.

tions of the data from curves based on Eqn. 6. For example, at both pHs, the low-MoS_4^{2-} data lie above the curves, while at intermediate MoS_4^{2-}, the data lie below the curves. A more elaborate model can be used to reduce these deviations. This model, represented by the dashed lines in Figure 7, is described by the following equation:

$$R^* = \frac{R^*_{m(1)}\,[MoS_4^{2-}]}{K_{1/2(1)} + [MoS_4^{2-}]} + \frac{R^*_{m(2)}\,[MoS_4^{2-}]^x}{K_{1/2(2)} + [MoS_4^{2-}]^x}\ \text{(constant pH)}. \tag{8}$$

As above, the equation for $R^{\ddagger}$ at pH 8.6 is identical in form. Here, x is the order with respect to MoS_4^{2-}. A value of $x > 1$ implies that the reactive surface intermediate is an oligomer. This model assumes that the reaction proceeds via a monomeric surface intermediate at low MoS_4^{2-} and also via an oligomeric intermediate at higher MoS_4^{2-} concentrations; formation of the oligomer occurs as follows:

$$\equiv S + xMoS_4^{2-} \leftrightarrow \equiv S - (MoS_4^{2-})_x. \tag{9}$$

Eqn. 8 contains five variable parameters; allowing all five to float produced unstable fits. To constrain the model, $R^*_{m(1)}$ and $R^*_{m(2)}$ were estimated visually by inspection of Figure 7, and values of $K_{1/2}$ were then obtained by fitting the data with x arbitrarily selected. For pH 8.6, we estimated that $R^{\ddagger}_{m(1)} = 3.5 \times 10^{-4}$ μmol h^{-1} m^{-2}, and $R^{\ddagger}_{m(2)} = 5.5 \times 10^{-4}$ μmol h^{-1} m^{-2}. Likewise, for pH 9.6, $R^*_{m(1)} = 1.5 \times 10^{-4}$ μmol h^{-1} m^{-2}, and $R^*_{m(2)} = 1.3 \times 10^{-4}$ μmol h^{-1} m^{-2}. Using these provisional values, we obtained satisfactory fits of the data at both pHs, shown as the dashed lines in Figure 7, only if $x \geq 4$. For $x = 4$, nonlinear regression on the data at pH 8.6 gives $K_{1/2(1)} = 13$ μmol/L and $K_{1/2(2)} = 7 \times 10^7$ μmol/L^4. For pH 9.6, $K_{1/2(1)} = 3$ μmol/L and $K_{1/2(2)} = 7 \times 10^6$ μmol/L^4. Uncertainties associated with the fitted parameters are 25 to 50%. Oligomers larger than tetramers cannot be ruled out because values of $x > 4$ give statistically similar fits. Values of $x < 4$ gave less satisfactory fits.

Making a confident choice between the monomer vs. monomer/oligomer models would require more extensive high-MoS_4^{2-} data than we have acquired. Since ΣMo in natural waters is usually $<10^{-7}$ mol/L, the second term in Eqn. 8 ordinarily will be negligible, and reaction pathways that proceed via oligomeric surface intermediates will not be important in nature. For this reason, we decided not to invest further research effort in the high-MoS_4^{2-} regime. For $\Sigma Mo < 10^{-7}$ mol/L, rates predicted by the monomer vs. monomer/oligomer models agree within approximately a factor of 3.

Using the simpler, monomer model, we can place an upper limit on the active site density on kaolinite's surface from the values of $K_{1/2}$ for pH 8.6 and 9.6 (250 and 20 μmol/L, respectively). Atomic absorption analysis of supernates from our slurries always revealed negligible (<5%) ΣMo loss from

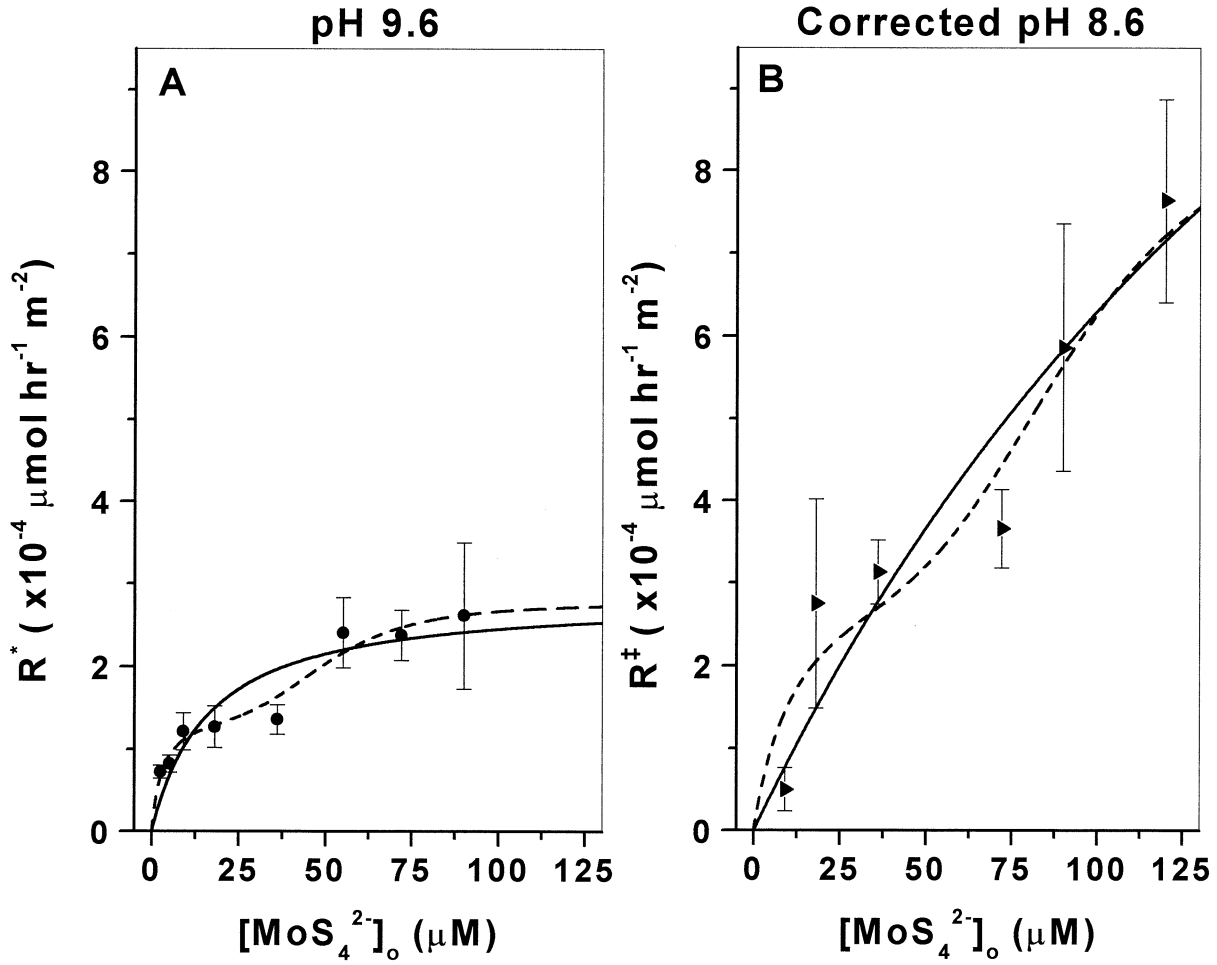

Fig. 7. Effect of initial MoS_4^{2-} concentration on R^*. Rates for pH 8.6 (denoted as $R^{\ddagger}$ on the y-axis) are corrected for the contribution of the high-pH mechanism to the reaction rate according to Eqn. 5. The solid curves were fit to Eqn. 6 with parameters given in the text. The dashed curves were fit to Eqn. 8 with x = 4 and parameters given in the text.

solution by adsorption to kaolinite. If <5% of 250 μmol/L or, in other words, <12.5 μmol/L Mo, saturates half the active sites on 469 m^2/L of kaolinite at pH 8.6, then the density of active sites is $<5.4 \times 10^{-8}$ mol of sites/m^2 or <0.03 sites/nm^2. For pH 9.6, the density of active sites is $<4.3 \times 10^{-9}$ mol of sites/m^2 or <0.003 sites/nm^2. These values may be compared to a total site density estimated to be 2 sites/nm^2 (Goldberg et al., 1998). Regardless of the uncertainties in these estimates, catalytically active sites apparently constitute a small minority of the total sites on the kaolinite surface at both pH 8.6 and 9.6. We therefore cannot exclude the possibility that active sites are associated with crystal anomalies such as point defects, dislocations, etc.

4.5. Effect of Electrolytes and PO_4^{3-}

Figure 8a compares the dependence of R^* on the ionic strength of NaCl vs. Na_2SO_4. In the dilute regime of the NaCl curve, the rate of hydrolysis increases by nearly twofold as ionic strength is increased from 0.9 to 10 mmol/L. A successive 10-fold rise in ionic strength reduces the rate to a value approximating that of the most dilute ionic strength. At 1 mol/L ionic strength, the rate falls to 40% of the rate of the dilute suspension. In contrast to NaCl, Na_2SO_4 always lowers the rate. The rate decreases by approximately 40% over the dilute portion of the Na_2SO_4 curve. Throughout the remaining 100-fold range of ionic strength, the rate of hydrolysis remains constant. In accord with the data presented in Figure 5, these results indicate that SO_4^{2-} and Cl^- affect rates in measurably different ways, but the magnitude of these changes is small considering the large concentration changes needed to produce them.

In contrast, Figure 8b shows the relationship between R^* and PO_4^{3-} concentration. The hydrolysis rate decreases by 50% with the addition of only 20 μmol/L PO_4^{3-}. Additional PO_4^{3-} diminishes the rate by a much smaller factor, suggesting that phosphate-binding sites are approaching saturation. Figure 8b demonstrates that PO_4^{3-}, at concentrations encountered in natural pore waters, effectively competes with MoS_4^{2-} for some of the active sites on the kaolin surface.

Hydrolysis rate reduction due to SO_4^{2-} and PO_4^{3-} indicates that these ions compete with MoS_4^{2-} for active sites on kaolinite even at the lowest concentrations tested. Both ions are

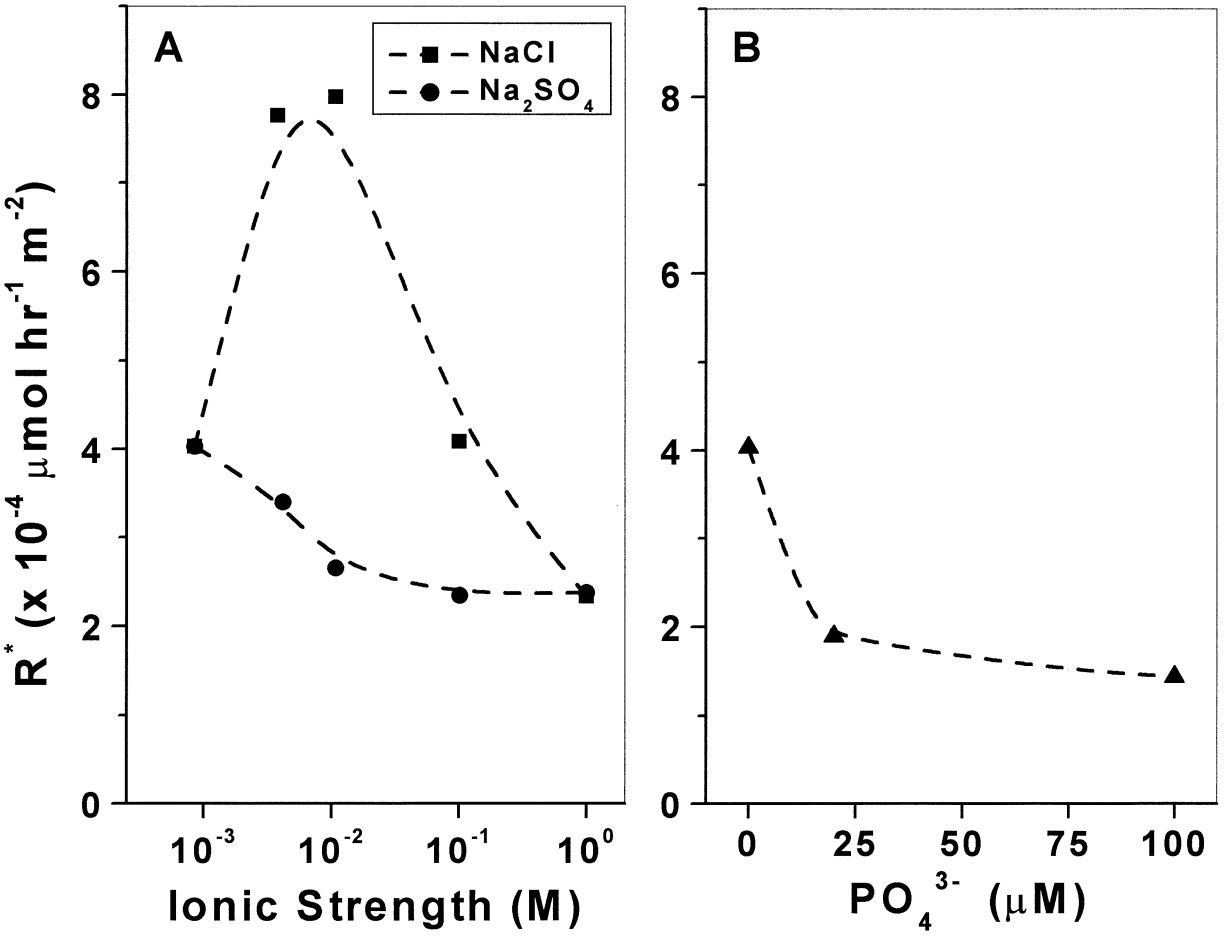

Fig. 8. Dependence of R^* on (A) the ionic strength of NaCl and Na_2SO_4 and (B) phosphate concentration. The lowest ionic strength ($\approx 10^{-3}$ mol/L) shown in (A) is the ionic strength of the buffered slurry with no salt added beyond pH adjust. Curves are spline interpolations. Conditions: MoS_4^{2-} (initial) = 18 μmol/L; B_T = 0.8 mmol/L; pH = 8.6; {kaolin} = 469 m^2/L.

known to adsorb and to associate with Al groups on kaolinite. Under mildly alkaline conditions, SO_4^{2-} adsorption is marginal, but PO_4^{3-} adsorption is substantial (He et al., 1997). A higher affinity of kaolinite for PO_4^{3-} explains why PO_4^{3-} is an effective inhibitor at lower concentrations than SO_4^{2-}.

The leachable phosphate content of KGa-1b was found to be approximately 3 μg P/g kaolin. A 38-g/L kaolin suspension, the highest concentration used in our experiments, would therefore release only 1 μmol/L PO_4^{3-}. Judging from Figure 8b, this amount of PO_4^{3-} is too small to produce a significant artifact in our kinetic experiments.

5. DISCUSSION

5.1. Mechanism of Oxide Catalyzed MoS_4^{2-} Hydrolysis

Constraints are placed on the mechanism by the following considerations. First, in the pH range of our experiments, MoO_4^{2-} is negligibly adsorbed to kaolinite (Goldberg et al., 1998). The well-known preference of Al and Si for O vs. S coordination suggests that thiomolybdates would not adsorb under conditions in which MoO_4^{2-} does not, and our limited evidence (Fig. 5b) supports this assumption. Second, nonetheless, hydrolysis of MoS_4^{2-} in our experiments involves kaolinite's surface in some critical way (Fig. 2). Evidence of site competition by very small concentrations of PO_4^{3-} and $MoOS_3^{2-}$ implies that hydrolysis requires formation of a specific, inner-sphere intermediate. Third, Figure 6 suggests that surface protons promote hydrolysis; on the other hand, persistence of surface catalysis to high pH, at which kaolinite is believed to be completely deprotonated (Huertas et al., 1998), suggests that surface protons are not essential. Fourth, most reactions of tetrahedral molybdate, and probably thiomolybdates, proceed through sixfold coordinated intermediates (You et al. 1986; Martire et al., 1989; see review by Erickson and Helz, 2000). Protonation of O or S coordinated to Mo^{VI} favors expansion of the coordination number from fourfold to sixfold through Mo's acceptance of nucleophiles (Honig and Kustin, 1972; Pope, 1983; Ozeki et al., 1996).

A plausible, monomeric mechanism applicable to the MoS_4^{2-} < 20 μmol/L, pH < 9 regime is illustrated in Figure 9. Initially, MoS_4^{2-} in the vicinity of the surface receives a proton from a surface ≡OH group. Thus activated, Mo undergoes nucleophilic attack by the $\equiv O^-$ group and by a water molecule, resulting in an inner-sphere, octahedral surface complex. This

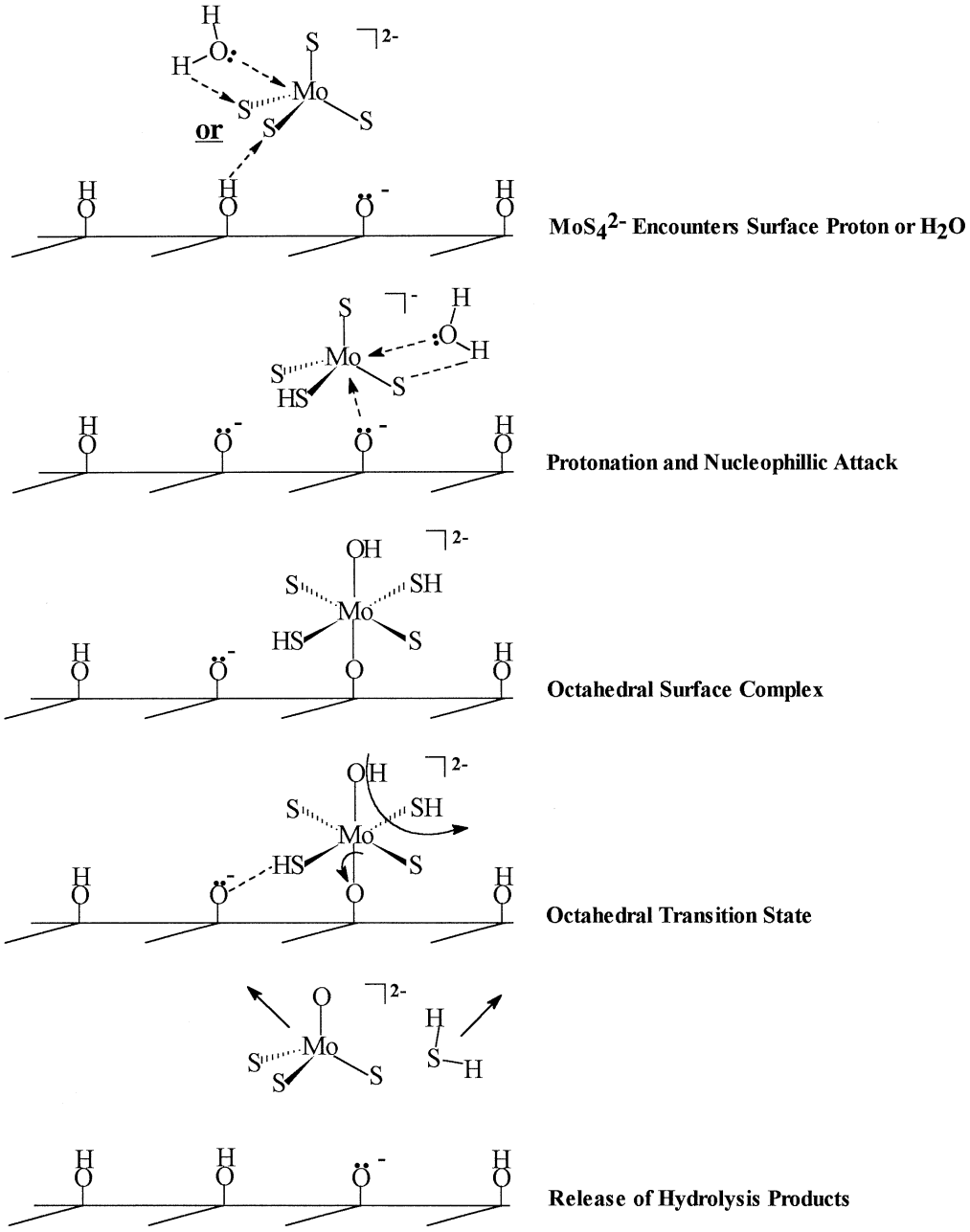

Fig. 9. Plausible monomeric mechanism of surface-catalyzed MoS_4^{2-} hydrolysis. The initial step of the mechanism illustrates the reaction pathways operating either below or above pH 9. Below pH 9, surface sites are the dominant proton donors to MoS_4^{2-}. Above pH 9, water is the dominant proton donor to MoS_4^{2-}; protonation is followed by addition of hydroxide ion.

complex is formed through proton-facilitated adsorption. Subsequent desorption and decomposition of this complex releases H_2S and $MoOS_3^{2-}$. The principal reaction pathway above pH 9 can be similar, but the initial proton must come from water, and a hyrdoxide ion, rather than a water molecule, must be added to $HMoS_4^-$ in the second step. This mechanism is consistent with the mechanism for aqueous-phase hydrolysis and sulfidation of $MoO_xS_{4-x}^{2-}$ anions advanced by Brule et al. (1988).

The mechanism in Figure 9 can work for any of the five anions in the $MoO_xS_{4-x}^{2-}$ series. Likewise, it can catalyze reactions in either direction (i.e., hydrolysis or sulfidization). Figure 9 portrays replacement of S by O in the first shell around Mo. To catalyze the reverse reaction, replacement of O by S, it is only necessary that on average, H_2S, rather than H_2O, enter the first shell during formation of the octahedral intermediate and that H_2O leave upon subsequent return to tetrahedral coordination. Statistically, this would occur when the H_2S concentration lies above the action point of the sulfide actuated geochemical switch of Erickson and Helz (2000).

Huertas et al. (1998) characterized surface sites on kaolinite

from titration data. Above pH 8, they found ≡Al-OH, ≡Al-O^- and ≡Si-O^- to be the principal species. Earlier, we concluded that the catalytically most active sites were minority sites. For the pH < 9 mechanism, acidity of the minority sites (pK_a ~ 9 from Fig. 6) is greater than for the majority ≡Al-OH sites (pK_a 10 to 11, from Huertas et al., 1998). Stronger acidity may partially account for the greater catalytic activity of the minority sites. It is plausible to propose that the catalytically most active sites in the pH 7.7 to 9 region are ≡Al-OH sites situated in special surface configurations that render them more acidic than the majority sites. Kawakami and Yoshida (1985) showed how the structural environments of ≡Al-OH groups modify their acidity. One possibility is that some of the catalytically most active sites are associated with defects or impurities. On the other hand, similar rates obtained in Figure 2b with hydrated δ-Al_2O_3, a synthetic product, and KGa-1b kaolinite, a natural product, point to the Al component of kaolinite, not to an extraneous mineral contaminant, as the source of catalytic activity.

Gilbert and Kustin (1976) described a number of parallel pathways that MoO_4^{2-} can follow in forming complexes with catechol derivatives. Forming catechol-molybdate complexes can be viewed as analogous to forming surface-molybdate complexes. The work of Gilbert and Kustin (1976) therefore reveals the potential complexity of $MoO_xS_{4-x}^{2-}$-surface interactions at the microscopic level. Figure 9 must be regarded as only illustrative of how these processes could occur. One point demonstrated by Gilbert and Kustin (1976) is that for protonated (probably octahedral) molybdate, rates of complex formation increase with the basicity of the ligand. Basicity of ≡Al-O^- groups on kaolinite surfaces is likely also to be an important determinant of MoS_4^{2-} hydrolysis rates.

The hint in Figure 7 that oligomeric intermediates also may be important in MoS_4^{2-} hydrolysis at higher MoS_4^{2-} concentrations is intriguing. Existence of surface oligomers on phyllosilicates, but not their role in catalysis, has been demonstrated by extended X-ray absorption fine structure in several systems (O'Day et al., 1994; Scheidegger et al., 1996).

Acidification of a solution containing ~10^{-5} mol/L MoS_4^{2-} (approximating MoS_4^{2-} in many of our experiments) will cause precipitation of amorphous MoS_3 beginning near pH 5. Amorphous MoS_3 is believed to contain Mo in octahedral coordination (Hibble et al., 1998). It is plausible to suggest that an oligomer resembling MoS_3 might nucleate epitaxially at acidic sites on kaolinite surfaces even when pH in the bulk solutions is mildly alkaline. As in the case of the monomeric mechanism presented in Figure 9, expansion of the first coordination number from 4 to 6 during formation of the oligomers and reversion of the coordination number to 4 upon dissolution could promote exchange of atoms in the first coordination sphere. However for this process to accomplish hydrolysis, it is necessary to assume that "MoS_3" oligomers incorporate some O in addition to S.

With increasing NaCl concentration, hydrolysis rates first accelerate and then diminish. For dilute NaCl, rate enhancement as ionic strength increases may result from contraction of the double layer, enhancing the ability of MoS_4^{2-} to diffuse to the negatively charged kaolinite surface against an electrostatic potential. At higher NaCl, the rate decrease might be due to replacement of surface coordinated protons by Na. Floccuation of kaolin particles, which decreases effective surface area, becomes important only above ~0.2 mol/L ionic strength (Novich and Ring, 1984). Acceleration of hydrolysis by low concentrations of NaCl supports an inner-sphere mechanism such as that in Figure 9. If hydrolysis involved an outer-sphere mechanism, rates should decline with increasing NaCl even in the low concentration regime because the electrolyte anion would compete with MoS_4^{2-} for access to the surface.

5.2. Will Surface Catalysis Be Important in Nature?

To determine whether mineral surfaces might be important in catalyzing $MoO_xS_{4-x}^{2-}$ transformations in nature, we calculate for idealized conditions the critical concentration of KGa-1b above which surface catalyzed hydrolysis exceeds aqueous phase hydrolysis. We assume that the only important reaction pathways in the aqueous phase are the H_3O^+ and H_2O catalyzed pathways, and we neglect possible pathways involving surface oligomers, because they should be negligible in dilute solutions. Under these conditions and pH < 9, Eqn. 3 can be written as

$$-\frac{d(MoS_4^{2-})}{dt} = (MoS_4^{2-})\left[6.7 \times 10^{-3}\ \text{mol/L s}^{-1}\ (H_3O^+) + 1.8 \times 10^{-11}\ \text{mol/L s}^{-1}\ (55.5\ \text{mol/L}) + (A)\frac{5.5 \times 10^{-13}\ \text{mol s}^{-1}\ \text{m}^{-2}}{2.5 \times 10^{-4}\ \text{mol/L} + (MoS_4^{2-})} + (A)\frac{8.3 \times 10^{-14}\ \text{mol s}^{-1}\ \text{m}^{-2}}{2.0 \times 10^{-5}\ \text{mol/L} + (MoS_4^{2-})}\right]. \quad (10)$$

The constants for the H_3O^+ and H_2O pathways are taken from Erickson and Helz (2000). From Eqn. 10, when $MoS_4^{2-} \ll$ 20 μmol/L (likely to be true in natural waters) and pH = 8.0, the threshold value of A is ~0.2 m^2/L. This much surface area is provided by only 10^{-2} g/L of KGa-1b. Thus, under the circumstances assumed in this calculation, surface catalysis would become dominant at quite modest concentrations of kaolinite (compare to Fig. 1). Including additional terms for buffer-catalyzed aqueous phase pathways in Eqn. 10 would force this estimate of A to be raised, but the arguments of Perdue and Wolfe (1983) suggest that the increase in A would be small.

The situation in real sediments is of course much more complicated than represented by this idealized calculation. Besides kaolinite, sediments contain other clay minerals having different properties (e.g., point of zero charge, specific surface area, affinity for thiomolybdates). Each mineral will influence rates differently. Sedimentary pore waters can contain various anions and cations that might affect surface-catalyzed reaction rates in the manner we have demonstrated for PO_4^{3-} and SO_4^{2-}. Dissolved silica and bicarbonate should be investigated because of their high abundance in pore waters. Sediments not only contain a large variety of mineral surfaces, but often, these are coated with organic materials. Organic materials may themselves be proton donors, but they also might block access of $MoO_xS_{4-x}^{2-}$ anions to catalytic sites on mineral surfaces. Mayer (1999) presents evidence that aluminosilicates in marine sediments present largely naked surfaces to pore waters, but the

extent to which even partial blockage by organic matter affects catalytic properties remains unknown.

Another issue concerns how compaction of sedimentary particles affects reaction dynamics in sediments. In this respect, it is interesting that in unsaturated soils, hydrolysis rates are sometimes observed to increase as relative humidity decreases (Xu, 1998). This counterintuitive response, in which water's reaction rate is increased by lowering its activity, is explained by arguing that in low-humidity soils, the solutes are confined to thin aqueous films on mineral surfaces. This proximity apparently enhances hydrolysis rates. Possibly, a similar effect occurs in compacted sediments.

This study was prompted by field evidence that Mo fixation occurs more readily in pore waters than in overlying waters. To help explain this behavior, we hypothesized that surfaces catalyze Mo(VI) transformations in nature. We have now proved this for the case of MoS_4^{2-} hydrolysis. The extent to which this process might be mitigated or negated by other effects in natural sediments and the extent to which other transformations involving thiomolybdates are affected are issues that must remain for the future.

Acknowledgments—This work was supported by the National Science Foundation (EAR-9980532) and the Maryland Water Resources Research Center, sponsored by the U.S. Geological Survey. We appreciate thoughtful reviews by Alan Stone, Yan Zheng, and an anonymous reviewer. G. R. Helz expresses his gratitude to his undergraduate mentor, Dick Holland, whose accomplishments as a teacher and scientist continually inspire.

Associate editor: P. A. O'Day

REFERENCES

Adelson J. M., Helz G. R., and Miller C. V. (2001) Reconstructing the rise of recent coastal anoxia; molybdenum in Chesapeake Bay sediments. *Geochim. Cosmochim. Acta* **65,** 237–252.

Al-Kanani T. and MacKenzie A. F. (1990) Pyrophosphate hydrolysis in mineral fractions of soils, goethite, kaolinite and montmorillonite. *Can. Soil Sci.* **149,** 239–247.

Bereznitski Y., Jaroniec M., and Maurice P. (1998) Adsorption characterization of two clay minerals society standard kaolinites. *J. Colloid Interface Sci.* **205,** 528–530.

Brule J. E., Hayden Y. T., Callahan K. P., and Edwards J. O. (1988) Equilibrium and rate constants for mononuclear oxythiomolybdate interconversions. *Gazz. Chim. Ital.* **118,** 93–99.

Clarke N. J. and Laurie S. H. (1987) Kinetics of the formation and hydrolysis reactions of some thiomolybdate(VI) anions in aqueous solution. *Inorg. Chim. Acta* **130,** 79–83.

Colodner D. (1991) *The Marine Geochemistry of Rhenium, Iridium, and Platinum*. Ph. D. thesis, Massachusetts Institute of Technology, Cambridge.

Crusius J., Pedersen T. F., Calvert S. E., Cowie G. L., and Oba T. (1999) A 35 kyr geochemical record from the Sea of Japan of organic matter flux variations and changes in intermediate water oxygen concentrations. *Paleoceanogr.* **14,** 248–259.

David D. J. (1968) The suppression of some interferences in the determination of molybdenum by atomic absorption spectroscopy. *Analyst* **93,** 79–82.

Dean W. E., Piper D. Z., and Peterson L. C. (1999) Molybdenum accumulation in Cariaco basin sediment over the past 24 k.y.: A record of water-column anoxia and climate. *Geology* **27,** 507–510.

Dean W. E., Gardner J. V., and Piper D. Z. (1997) Inorganic geochemical indicators of glacial-interglacial changes in productivity and anoxia on the California continental margin. *Geochim. Cosmochim. Acta* **61,** 4507–4518.

El-Amamy M. M. and Mill T. (1984) Hydrolysis kinetics of organic chemicals on montmorillonite and kaolinite surfaces as related to moisture content. *Clays Clay Miner.* **32,** 67–73.

Emerson S. R. and Huested S. S. (1991) Ocean anoxia and the concentrations of molybdenum and vanadium in seawater. *Mar. Chem.* **34,** 177–186.

Eng P. J., Trainor T. P., Brown G. E., Jr., Waychunas G. A., Newville M., Sutton S. R., and Rivers M. L. (2000) Structure of the hydrated a-Al_2O_3 (0001) surface. *Science* **288,** 1029–1033.

Erickson B. E. (1997) *The Speciation of Molybdenum in Sulfidic Natural Waters*. Ph. D. thesis, University of Maryland, College Park.

Erickson B. E. and Helz G. R. (2000) Molybdenum(VI) speciation in sulfidic waters: Stability and lability of thiomolybdates. *Geochim. Cosmochim. Acta* **64,** 1149–1158.

Francois R. (1988) A study on the regulation of the concentrations of some trace elements (Rb, Sr, Zn, Pb, Cu, V, Cr, Ni, Mn and Mo) in Saanich Inlet sediments, Br. Columbia. *Mar. Geol.* **83,** 285–308.

Gilbert K. and Kustin K. (1976) Kinetics and mechanism of molybdate and tungstate complex formation with catechol derivatives. *J. Am. Chem. Soc.* **98,** 5502–5512.

Goldberg S., Su C., and Forster H. S. (1998) Sorption of molybdenum on oxides, clay minerals and soils. In *Adsorption of Metals by Geomedia* (ed. E. A. Jenne), chap. 19. Academic Press, San Diego, CA.

Greenberg A. E., Clesceri L. S., and Eaton A. D., eds. (1992) *Standard Methods for the Examination of Water and Wastewater*. American Public Health Association, Washington, DC.

Griffin J. J., Windom, H., and Goldberg E. D. (1968) The distribution of clay minerals in the World Ocean. *Deep-Sea Res.* **15,** 433–459.

He L. M., Zelazny L. W., Baligar V. C., Ritchey K. D., and Martens D. C. (1997) Ionic strength effects on sulfate and phosphate adsorption on γ-alumina and kaolinite: Triple-layer model. *Soil Sci. Soc. Am. J.* **61,** 784–793.

Helz G. R., Miller C. V., Charnock J. M., Mosselmans J. F. W., Pattrick R. A. D., Garner C. D., and Vaughan D. J. (1996) Mechanism of molybdenum removal from the sea and its concentration in black shales: EXAFS evidence. *Geochim. Cosmochim. Acta* **60,** 3631–3642.

Hibble S. J., Walton R. I., Pickup D. M., and Hannon A. C. (1998) Amorphous MoS_3: Clusters or chains? The structural evidence. *J. Non-Cryst. Solids* **232–234,** 434–439.

Holland H. D. (1984) *The Chemical Evolution of the Atmosphere and Oceans*. Princeton University Press, Princeton, NJ.

Honig D. S. and Kustin K. (1972) Relaxation spectra of molybdate polymers in aqueous solution. *J. Phys. Chem.* **76,** 1575–1578.

Huertas F. J., Chou L., and Wollast R. (1998) Mechanism of kaolinite dissolution at room temperature and pressure: Part 1. Surface speciation. *Geochim. Cosmochim. Acta* **62,** 417–431.

Jencks W. P. (1969) *Catalysis in Chemistry and Enzymology*. Dover, New York.

Kawakami H. and Yoshida S. (1985) Quantum-chemical studies of alumina: Part 1. Brønsted acidity and basicity. *J. Chem. Soc., Faraday Trans.* **81,** 1117–1127.

Laidler, K. J. (1987) *Chemical Kinetics*, 3rd ed. Harper & Row, New York.

Laurie S. H., Pratt D. E., and Yong J. H. L. (1984) Preparation and properties of the sodium salt of tetrathiomolybdate(VI), $Na_2MoS_4 \cdot 3.5H_2O$. *Inorg. Chim. Acta* **93,** L57–L59.

Martire D. O., Feliz M. R., and Capparelli A. L. (1989) Linear enthalpy correlation in molybdenum(VI) octahedral substitutions. *Polyhedron* **8,** 1387–1389.

Mayer L. M. (1999) Extent of coverage of mineral surfaces by organic matter in marine sediments. *Geochim. Cosmochim. Acta* **63,** 207–215.

Mingelgrin U., Saltzman S., and Yaron B. (1977) A possible model for the surface-induced hydrolysis of organophosphorus pesticides on kaolinite clays. *Soil Sci. Am. Proc.* **41,** 519–523.

Mingelgrin U. and Saltzman S. (1979) Surface reactions of parathion on clays. *Clays Clay Miner.* **27,** 72–78.

Morford J. L. and Emerson S. (1999) The geochemistry of redox sensitive trace metals in sediments. *Geochim. Cosmochim. Acta* **63,** 1735–1750.

Novich B. E. and Ring T. A. (1984) Colloid stability of clays using proton correlation spectroscopy. *Clays Clay Miner.* **32,** 400–406.

O'Day P. A., Parks G. A., and Brown G. E., Jr. (1994) Molecular structure and binding sites of cobalt(II) surface complexes on kaolinite from x-ray absorption spectroscopy. *Clays Clay Miner.* **42,** 337–355.

Ozeki T., Adachi H., and Shigero I. (1996) Estimation of the dissolved structures and condensation reactivities of mononuclear molybdenum(VI) species in solution using the UV-vis absorption spectra and molecular orbital calculation DV-Xα. *Bull. Chem. Soc. Jpn.* **69,** 619–625.

Perdue E. M. and Wolfe N. L. (1983) Prediction of buffer catalysis in field and laboratory studies of pollutant hydrolysis reactions. *Environ. Sci. Technol.* **17,** 635–642.

Pope M. T. (1983) *Heteropoly and Isopoly Oxometalates*. Springer Verlag, Berlin, Germany.

Pruett R. J. and Webb H. L. (1993) Sampling and analysis of KGa-1B well-crystallized kaolin source clay. *Clays Clay Miner.* **41,** 514–519.

Saltzman S., Yaron B., and Mingelgrin U. (1974) The surface catalyzed hydrolysis of parathion on kaolinite. *Soil Sci. Soc. Am. Proc.* **38,** 231–234.

Scheidegger A. M., Lamble G. M., and Sparks D. L. (1996) Investigation of Ni sorption on pyrophyllite: An XAFS study. *Environ. Sci. Technol.* **30,** 548–555.

Schindler P. W. and Stumm W. (1987) The surface chemistry of oxides, hydoxides and oxide minerals. In *Aquatic Surface Chemistry* (ed. W. Stumm), chap. 4. John Wiley, New York.

Sutheimer S. H., Maurice P. A., and Zhou Q. (1999) Dissolution of well and poorly crystallized kaolinites: Al speciation and effects of surface characteristics. *Am. Mineral.* **84,** 620–628.

Vorlicek, T. P. (in preparation) *Mineral Catalysis of Tetrathiomolybdate Hydrolysis and Iron Scavenging Reactions of Molybdenum*. Ph.D. thesis, University of Maryland, College Park.

Wang M. C. and Huang P. M. (1989) Catalytic power of nontronite, kaolinite and quartz and their reaction sites in the formation of hydroquinone-derived polymers. *Appl. Clay Sci.* **4,** 43–57.

Xu S. (1998) Hydrolysis of poly(dimethylsiloxanes) on clay minerals as influenced by exchangeable cations and moisture. *Environ. Sci. Technol.* **32,** 3162–3168.

Yarincik K. M., Murray R. W., Lyons T. W., Peterson L. C., and Haug G. H. (2000) Oxygenation history of bottom waters in the Cariaco basin, Venezuela, over the past 578,000 years. Results from redox-sensitive metals (Mo, V, Mn, Fe). *Paleoceanogr.* **15,** 593–604.

You J. F., Wu D., and Liu H. Q. (1986) Electrochemical studies of molybdate and thiomolybdates. *Tetrahedron* **5,** 535–537.

Young, J. R. (1981) *A Study of the Adsorption of Nickel(II) Onto an Amorphous Silica Surface by Chemical and NMR Methods*. Ph.D. thesis, California Institute of Technology, Pasadena.

Zamaraev K. I, Romannikov V. N., Salganik R. I., Wlassoff W. A., and Khramtsov V. V. (1997) Modeling of the prebiotic synthesis of oligopeptides: Silicate catalysts help to overcome the critical stage. *Origins Life Evol. Biosphere* **27,** 325–337.

Zheng Y., Anderson, R. F., Van Geen A., and Kuwabara J. (2000) Authigenic molybdenum formation in marine sediments: A link to pore water sulfide in the Santa Barbara Basin. *Geochim. Cosmochim. Acta* **64,** 4165–4178.

Zhou Q. (1996) *Surface Characteristics and Dissolution Kinetics of Two Standard Kaolinites*. Master's thesis, Kent State University, Kent, OH.